Testing cosmology with cosmic sound waves

Pier Stefano Corasaniti[1] and Alessandro Melchiorri[2,3]

[1]*LUTH, Observatoire de Paris, CNRS UMR 8102, Université Paris Diderot, 5 Place Jules Janssen, 92195 Meudon Cedex, France*
[2]*Dipartimento di Fisica e Sezione INFN, Universita' degli Studi di Roma "La Sapienza", Ple Aldo Moro 5,00185, Rome, Italy*
[3]*CERN, Theory Division, CH-1211 Geneva 23, Switzerland*

(Received 30 November 2007; published 9 May 2008)

Wilkinson Microwave Anisotropy Probe (WMAP) observations have accurately determined the position of the first two peaks and dips in the cosmic microwave background (CMB) temperature power spectrum. These encode information on the ratio of the distance to the last scattering surface to the sound horizon at decoupling. However prerecombination processes can contaminate this distance information. In order to assess the amplitude of these effects, we use the WMAP data and evaluate the relative differences of the CMB peak and dip multipoles. We find that the position of the first peak is largely displaced with respect to the expected position of the sound horizon scale at decoupling. In contrast, the relative spacings of the higher extrema are statistically consistent with those expected from perfect harmonic oscillations. This provides evidence for a scale dependent phase shift of the CMB oscillations which is caused by gravitational driving forces affecting the propagation of sound waves before recombination. By accounting for these effects we have performed a Markov Chain Monte Carlo likelihood analysis of the location of WMAP extrema to constrain, in combination with recent BAO data, a constant dark energy equation of state parameter w. For a flat universe we find a strong 2σ upper limit $w < -1.10$, and including the Hubble Space Telescope prior, we obtain $w < -1.14$, which is only marginally consistent with limits derived from the Supernova Legacy Survey sample. On the other hand, we infer larger limits for nonflat cosmologies. From the full CMB likelihood analysis, we also estimate the values of the shift parameter R and the multipole l_a of the acoustic horizon at decoupling for several cosmologies, to test their dependence on model assumptions. Although the analysis of the full CMB spectra should always be preferred, using the position of the CMB peaks and dips provides a simple and consistent method for combining CMB constraints with other data sets.

DOI: 10.1103/PhysRevD.77.103507 PACS numbers: 98.80.Es, 95.36.+x

I. INTRODUCTION

Cosmic microwave background (CMB) observations have provided crucial insights into the origin and evolution of present structures in the universe [1–3]. Physical processes that occurred before, during, and after recombination have left distinctive signatures on the CMB. The most prominent feature is a series of peaks and dips in the anisotropy power spectrum, the remnant imprints of acoustic waves propagating in the primordial photon-baryon plasma at the time of decoupling [4–6]. This oscillatory pattern carries specific information about several cosmological parameters [7]. As an example, the angular scale at which these oscillations are observed provides a distance measurement of the last scattering surface to the sound horizon at decoupling, and hence a clean test of cosmic curvature [8].

Observations from the Wilkinson Microwave Anisotropy Probe (WMAP) satellite have accurately detected the peak structure of the CMB power spectrum. These data have constrained the geometry of the universe to be nearly flat and have precisely determined other cosmological parameters [9]. On the other hand, constraints on dark energy are less stringent; this is because its late time effects leave a weaker imprint of the CMB, which is diluted by degeneracies with other parameters. Indeed, other cosmological tests can be more sensitive to the signature of dark energy; nonetheless, they still require additional information from CMB to break the parameter degeneracies. As an example, CMB constraints are usually combined with those from supernova type Ia (SN Ia) luminosity distance data. Alternatively, the CMB can be used in combination with measurements of the baryon acoustic oscillations (BAO) in the galaxy power spectrum [10]. In fact, the same acoustic signature present in the CMB is also imprinted in the large scale distribution of the galaxy, thus providing a complementary probe of cosmic distances at lower redshifts.

A likelihood analysis of the CMB spectra is certainly the more robust approach to implement CMB constraints with those from other data sets. This can be very time consuming; henceforth, one can try to compress the CMB information into a few measurable and easily computable quantities. Recent literature has focused on the use of the shift parameter R, and the multipole of the acoustic scale at decoupling l_a [11,12]. However, these quantities are not directly measured by CMB observations; they are inferred as secondary parameters from the cosmological constraints obtained from the full CMB likelihood analysis. Consequently their use as *data* can potentially lead to

 © 2008 The American Physical Society

results which suffer from model dependencies, as well as prior parameter assumptions made in the analysis from which the values of R (l_a) have been inferred in the first place. In contrast the multipole location of the CMB extrema can be directly determined from the observed temperature power spectrum through model-independent curve fitting. These measurements can then be used to constrain cosmological parameters provide that prerecombination corrections are properly taken into account.

In this paper we analyze in detail the cosmological information encoded in the position of the CMB extrema as measured by WMAP. Our aim is to provide a simple and unbiased method for incorporating CMB constraints into other data sets, which is an alternative to that of using R and/or l_a [11,12]. First we estimate the amplitude of prerecombination mechanisms that can displace the location of the CMB extrema with respect to the angular scale of the sound horizon at decoupling. In particular, we show that the WMAP location of the first peak is strongly affected by such mechanisms, while the displacements induced on the higher peaks and dips are smaller. By accounting for these effects we perform a cosmological parameter analysis and infer constraints on dark energy under different prior assumptions, including the cosmic curvature. We then combine these results with measurements of BAO from the Sloan Digital Sky Survey (SDSS) and 2-degree field (2dF) data [13], and confront the inferred constraints with those obtained using SN Ia data from the Supernova Legacy Survey (SNLS) [14]. Finally we test for potential model dependencies of R (and l_a) by performing a full likelihood analysis of the WMAP spectra for different sets of cosmological parameters.

The paper is organized as follows: in Sec. II we review the physics of the CMB acoustic oscillations. In Sec. III we discuss the relative shifts of the multipoles of the WMAP peaks and dips. In Sec. IV we present the results of the cosmological parameter inference using the location of the CMB extrema in combination with BAO. In Sec. V we confront the results with the SN Ia likelihood analysis from the Supernova Legacy Survey (SNLS) sample. We discuss the results on the shift parameter in Sec. VI and present our conclusions in Sec. VII.

II. CMB ACOUSTIC OSCILLATIONS

The onset of acoustic waves on the subhorizon scales of the tightly coupled photon-baryon plasma before recombination is a natural consequence of photon pressure resisting gravitational collapse. The properties of these oscillations depend both on the background expansion and the evolution of the gravitational potentials associated with the perturbations present in the system. In the following we will briefly review the basic processes which affect the propagation of these waves before decoupling. Interested readers will find more detailed discussions in [6,7]. Let us consider the photon temperature fluctuation $\Theta_0 \equiv \Delta T$ (monopole); following Hu and Sugiyama [6] its evolution is described by

$$\ddot{\Theta}_0 + \frac{\dot{R}}{1+R}\dot{\Theta}_0 + k^2 c_s^2 \Theta_0 = F(\eta), \tag{1}$$

where the dot is the derivative with respect to conformal time, $R = 3\rho_b/4\rho_\gamma$ is the baryon-to-photon ratio, k is the wave number, and $c_s = c/\sqrt{3(1+R)}$ is the sound speed of the system with c the speed of light. The source term

$$F = -\ddot{\Phi} - \frac{\dot{R}}{1+R}\dot{\Phi} - k^2\frac{\Psi}{3} \tag{2}$$

represents a driving force, where Φ and Ψ are the gauge-invariant metric perturbations, respectively.

During recombination the sound speed is slowly varying; in such a case it is easy to see from Eq. (1) that the homogeneous equation ($F = 0$) admits oscillating solutions of the form

$$\Theta_0^{\rm hom}(\eta) = A_1 \cos k r_s(\eta) + \frac{A_2}{k}\sin k r_s(\eta) \tag{3}$$

where A_1 and A_2 are set by the initial conditions and $r_s(\eta) = \int_0^\eta c_s(\eta')d\eta'$ is the sound horizon at time η. At the time of decoupling, η_*, the positive and negative extrema of these oscillations appear as a series of peaks in the anisotropy power spectrum. Their location in the multipole space is a multiple integer of the inverse of the angle subtended by the sound horizon scale at decoupling, namely, $l_m^{\rm peak} = m l_a$ with $m = 1, 2, \ldots$ and

$$l_a = \pi\frac{r_K(z_*)}{r_s(z_*)}, \tag{4}$$

where z_* is the recombination redshift and $r(z)$ the comoving distance to z,

$$r_K(z) = \frac{c}{H_0}\frac{1}{\sqrt{|\Omega_K|}} f\left(\sqrt{|\Omega_K|} I(z)\right), \tag{5}$$

with H_0 the Hubble constant, $|\Omega_K| = -K/H_0^2$ with K the constant curvature, $f(x) = \sin(x), \sinh(x), x$ for $K > 0$, $K < 0$, and $K = 0$, respectively, and $I(z) = \int_0^z dz' H_0/H(z')$.

Scales for which the monopole vanishes also contribute to the anisotropy power spectrum. In such a case the signal comes from the nonvanishing photon velocity Θ_1 (dipole) which oscillates with a phase shifted by $\pi/2$ with respect to the monopole [6]. Therefore photons coming from these regions are responsible for a series of troughs in the anisotropy power spectrum at multipoles $l_n^{\rm dip} = n l_a$ with $n = m + 1/2$.

The full solution to Eq. (1) at decoupling reads as [15]

$$\Theta_0(\eta_*) = \Theta_0^{\rm hom}(\eta_*) + \frac{A_3}{k}\int_0^{\eta_*} d\eta' [1 + R(\eta')]^{3/4} \times \sin[k r_s(\eta_*) - k r_s(\eta')] F(\eta'), \tag{6}$$

where A_3 is set by the initial conditions. As we can see from Eq. (6), including the driving force F induces a scale dependent phase shift of the acoustic oscillations, which is primarily caused by the time variation of the gravitational potential Φ. In fact, perturbations on scales which enter the horizon at the matter-radiation equality experience a variation of the expansion rate which causes a time evolution of the associated gravitational potentials. This mechanism is dominant on the large scales and is responsible for the so-called early integrated Sachs-Wolfe (ISW) effect [16]. The overall effect is to displace the acoustic oscillations with respect to the pure harmonic series. For a spectrum of adiabatic perturbations we may expect this displacement to become negligible on higher harmonics since the gravitational potentials decay as $\Phi \propto (k\eta)^{-2}$ on scales well inside the horizon. This is not the case if active perturbations were present on such scales before the epoch of decoupling.

In order to account for these prerecombination effects, a realistic modeling of the multipole position of the CMB maxima and minima is given by [17]

$$l_m = l_a(m - \varphi_m), \tag{7}$$

where $m = 1, 2, \ldots$ for peaks and $m = 3/2, 5/2, \ldots$ for dips; φ_m parametrizes the displacement caused by the driving force. Because of the scale dependent nature of the driving effect discussed above, it is convenient to decompose the correction term as $\varphi_m = \bar{\varphi} + \delta\varphi_m$, where $\bar{\varphi} \equiv \varphi_1$ is the overall shift of the first peak with respect to the sound horizon, and $\delta\varphi_m$ is the shift of the mth extrema relative to the first peak [18].

It is worth noticing that the relative spacing of the CMB peaks and dips is independent of the geometry and late time expansion of the universe, and it is only sensitive to prerecombination physics.

III. PHASE SHIFT OF WMAP PEAKS AND DIPS

WMAP observations have provided an accurate determination of the CMB power spectrum. The multipoles of the CMB extrema have been inferred using a functional fit to the uncorrelated band powers as described in [19]. Hinshaw *et al.* [3] have applied this method to the WMAP 3-year data and found the position of the first two peaks and dips to be at $l_1 = 220.8 \pm 0.7$, $l_{3/2} = 412.4 \pm 1.9$, $l_2 = 530.9 \pm 3.8$, and $l_{5/2} = 675.2 \pm 11.1$, respectively.

We want to determine whether these measurements provide any evidence for driving effects affecting the acoustic oscillations. In order to do so, we evaluate the relative spacings between the WMAP measured mth and m'th extrema,

$$\Delta_{m,m'} = \frac{l_{m'}}{l_m} - 1, \tag{9}$$

and the propagated errors $\sigma_{\Delta_{m,m'}}$.

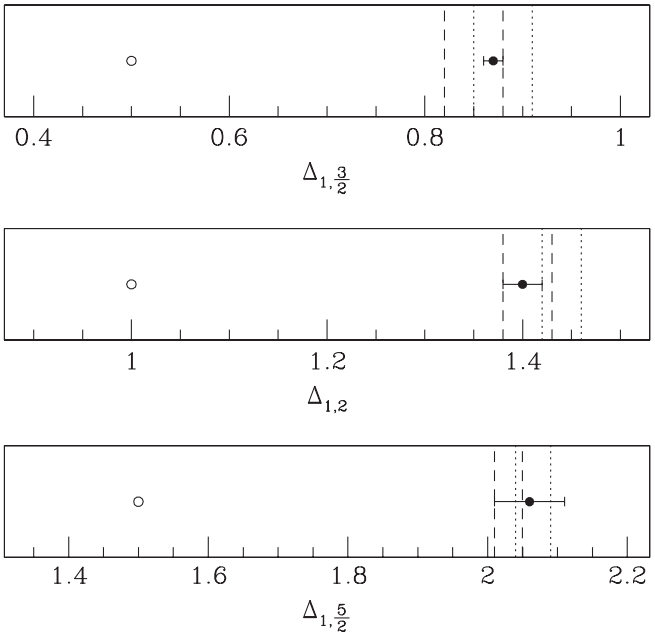

FIG. 1. WMAP spacings of $l_{3/2}$, l_2, and $l_{5/2}$ relative to l_1 (black solid circles) and propagated errors. The values expected from the harmonic series are $\Delta_{1,3/2} = 1/2$, $\Delta_{1,2} = 1$, and $\Delta_{1,5/2} = 3/2$ (open circles). Vertical dashed lines delimit the expected interval of variation of the relative spacings obtained by including the shift corrections as parametrized in [18] and evaluated over a conservative range of cosmological parameter values (see text). The dotted vertical lines include the effect of three massless neutrinos.

Let us first consider the spacings relative to the location of the first peak. We find $\Delta_{1,3/2} = 0.87 \pm 0.01$, $\Delta_{1,2} = 1.40 \pm 0.02$, and $\Delta_{1,5/2} = 2.06 \pm 0.05$, respectively. These estimates are shown in Fig. 1 (black solid circles), where we also plot the relative spacings as expected from a sequence of perfect acoustic oscillations (open circles). It is evident that the WMAP inferred values of $\Delta_{1,m}$ lie many sigmas away from those expected from the harmonic series. This provides clear evidence that the position of the first peak is largely affected by the driving force at decoupling. Such a large displacement is most likely caused by the early ISW, although an additional contribution from isocurvature fluctuations [20] or active gravitational potentials [21] cannot be excluded.

Let us focus now on the displacement of the second peak relative to the first one; since $\Delta_{1,2} > 1$ it follows that $\bar{\varphi} > \delta\varphi_2$. This implies that the overall shift of l_1 with respect to l_a is larger than the shift of l_2 relative to l_1. As discussed in the previous section this is consistent with having the gravitational potentials inside the sound horizon scaling as $\Phi \propto (k\eta)^{-2}$, thus inducing a weaker driving force. This can be seen more clearly in Fig. 2, where we plot $\Delta_{3/2,2}$, $\Delta_{2,5/2}$, and $\Delta_{3/2,5/2}$.

Apart from $\Delta_{2,3/2} = 0.29 \pm 0.01$, whose value suggests the presence of a non-negligible driving effect still on the

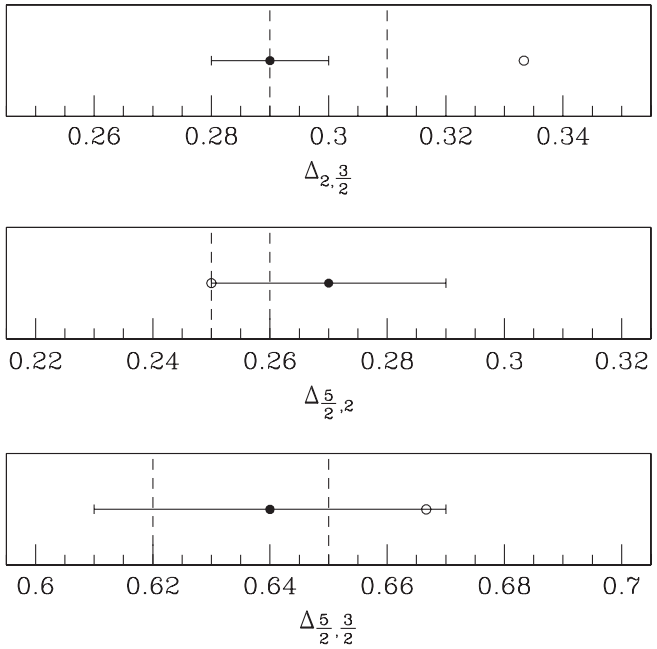

FIG. 2. As in Fig. 1 for $l_{3/2}$, l_2, and $l_{5/2}$ relative spacings. The harmonic series values are $\Delta_{3/2,2} = 1/3$, $\Delta_{2,5/2} = 1/4$, and $\Delta_{3/2,5/2} = 2/3$.

scale of the first dip, we may notice that all other spacings are statistically consistent with the prediction of the harmonic series.

Therefore these results suggest the existence of a scale dependent phase shift of the CMB acoustic oscillations. The effect is larger on the scale of the first acoustic peak, while it is weaker for the higher harmonics. The upcoming Planck mission will map more accurately the location of the higher peaks and dips and provide a cleaner detection of this shift.

Indeed, driving effects are well accounted for by the CMB theory as incorporated in standard Boltzmann codes [22]. For instance, a standard adiabatic spectrum of initial density perturbations leads to phase shifts which are consistent with those we have inferred here. To show this we have used the fitting formulas provided in [18] for adiabatic models which parametrize φ_m in terms of the total matter density $\Omega_m h^2$, the baryon density $\Omega_b h^2$, the dark energy density at decoupling $\Omega_{\rm DE}^{\rm dec}$, and the scalar spectral index n_s. Assuming $\Omega_{\rm DE}^{\rm dec} = 0$ we evaluate these formulas over the following range of parameter values, $0.08 < \Omega_m h^2 < 0.11$, $0.020 < \Omega_b h^2 < 0.024$, $0.92 < n_s < 1.1$, and infer the corresponding intervals for the relative spacings $\Delta_{m,m'}$. These are drawn in Figs. 1 and 2 as vertical dashed lines. It can be seen that these intervals are statistically consistent with the measured spacings. Including the contribution of three massless neutrinos (dotted vertical lines) slightly shifts the $\Delta_{1,m}$ intervals further from the expected values of the perfect harmonic oscillator. This is because the presence of relativistic neutrinos extends the radiation era and therefore leads to a more effective early ISW effect on large scales. In contrast we find no differences for the intervals of the other peak and dip spacings.

IV. PARAMETER INFERENCE

We perform a Markov Chain Monte Carlo (MCMC) likelihood analysis to derive cosmological parameter constraints using the measurements of the WMAP extrema discussed in the previous section. Again we account for the shift corrections by evaluating the model prediction for l_m using Eq. (7), with the displacements φ_m parametrized as in [18]. We compute the recombination redshift z_* using the fitting formulas provided in [23]. Cosmological constraints derived from the location of the CMB peaks have been presented in previous works (e.g. [24–26]). Here our aim is to derive bounds on dark energy which are independent of supernova Ia data and rely only on the cosmic distance information encoded in the angular scale of the sound horizon as inferred from the multipole position of the WMAP peaks and dips, and BAO measurements.

First we consider flat models with dark energy parametrized by a constant equation of state w. We then test the stability of the inferred constraints by extending the analysis to models with nonvanishing curvature, $\Omega_k \neq 0$. We also consider flat dark energy models with a time varying equation of state parametrized as $w = w_0 + w_1(1 - a)$, the Chevallier-Polarski-Linder (CPL) parametrization [27,28]. We want to remark that for models with $w_1 \gg 1$, the dark energy density can be non-negligible at early times. Therefore, in order to consistently account for the shifts induced on the location of the CMB peaks and dips, we compute for each model in the chain the corresponding value of $\Omega_{\rm DE}^{\rm dec}$ so as to include its value in the shift fitting formulas.

The credible intervals on the parameters of interest are inferred after marginalizing over h, $\Omega_b h^2$, and n_s, respectively. We let them vary in the following intervals: $0.40 < h < 1.00$, $0.020 < \Omega_b h^2 < 0.024$, and $0.94 < n_s < 1.10$. Marginalizing over these parameters is necessary due to the parameter degeneracies in r_K, r_s, and to properly account for the shift corrections φ_m.

As a complementary data set we use the cosmic distance as inferred from the BAO in the SDSS and 2dF surveys [13]. These measurements consists of the ratio $r_s(z_*)/D_V(z)$, where $D_V(z)$ is a distance measure given by

$$D_V(z) = [(1 + z)^2 D_A(z) cz/H(z)]^{1/3}, \qquad (10)$$

with $D_A(z) = r_K(z)/(1 + z)$ the angular diameter distance at z. In particular, Percival *et al.* [13] have found $D_V(0.35)/D_V(0.2) = 1.812 \pm 0.060$.

In order to reduce the degeneracy with the Hubble parameter, we also infer constraints assuming a Gaussian prior, $h = 0.72 \pm 0.08$, as inferred from the Hubble Space Telescope (HST) project [29]. In Fig. 3 we plot the margi-

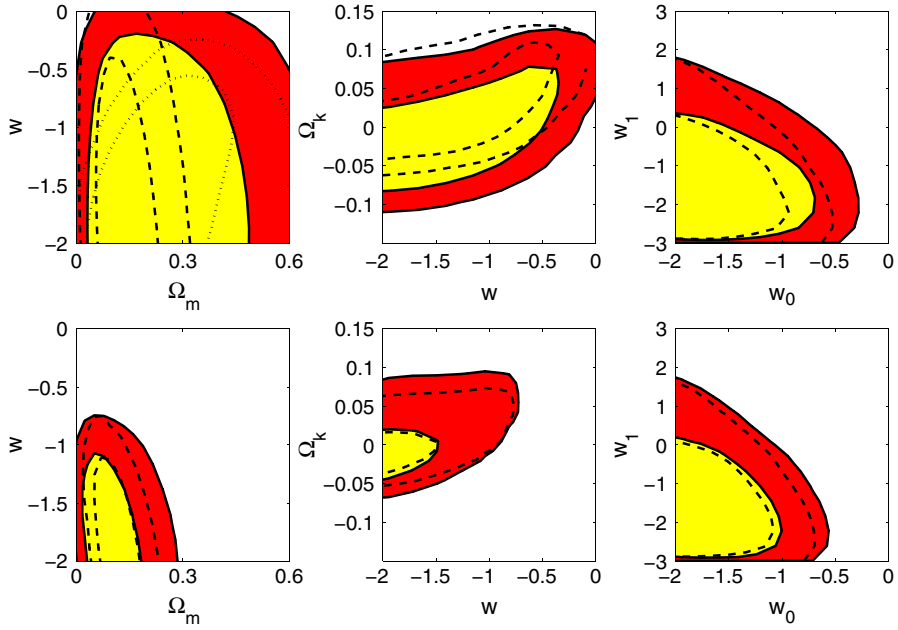

FIG. 3 (color online). Marginalized 1σ and 2σ likelihood contours from WMAP extrema (upper panels) and in combination with BAO (lower panels). Dashed lines correspond to contours inferred under HST priors. The dotted lines in the upper left panel correspond to limits inferred assuming $\Omega_b = 0.023$ and $n_s = 0.96$.

nalized 1σ and 2σ contours in the Ω_m- w, w- Ω_K, and w_0- w_1 planes, respectively. The upper panels correspond to constraints inferred from WMAP extrema alone, while the lower panels include the BAO data. Dashed contours are inferred under the HST prior. To be conservative, we only quote marginalized 2σ limits. We now discuss these results in more detail.

A. Limits from CMB peaks and dips

As it can be seen in Fig. 3 (upper left panel) the CMB extrema alone poorly constrain the Ω_m-w plane. In particular, the 1σ and 2σ regions are larger than those obtained from the WMAP analysis [9]. This is because, due to the late ISW effect, more information about dark energy is contained in the full CMB spectrum than just in the distance to the last scattering surface as encoded in the position of the CMB peaks and dips. Besides, several degeneracies with other parameters are strongly reduced. A direct consequence of this is that our limits on w are unbounded from below. After marginalizing over all parameters we find $\Omega_m = 0.29^{+0.41}_{-0.23}$ and $w < -0.18$ at 2σ. A model with $\Omega_m = 1$ is consistent at the 95% confidence level with the location of the WMAP extrema provided that $h \approx 0.42$. This is in agreement with the results presented in [30]. On the other hand, imposing an HST prior (dash contours) reduces the degeneracy in the Ω_m- w plane, and the marginalized 2σ limits are $\Omega_m = 0.16^{+0.15}_{-0.11}$ and $w < -0.25$, respectively. The upper limit on w improves if a strong prior on $\Omega_b h^2$ and n_s is assumed (dotted contours in the upper left panel). As an example, imposing $\Omega_b h^2 = 0.0223$ and $n_s = 0.96$, we find $w < -0.65$ at 2σ. Indeed, using the analysis of the full CMB power spectrum provides better constraints. For instance, in Fig. 4 we plot the 1σ and 2σ contours inferred from a MCMC likelihood analysis of the WMAP 3-year spectra in combination with the HST prior. The limits are more stringent than in the previous case. This is because the amplitude of the first peak as well as the relative amplitude of the other peaks are particularly sensitive to Ω_m, Ω_b, and h. Hence, degeneracies contributing to the uncertainties in the Ω_m-w plane are further reduced. As mentioned before, a robust dark energy parameter inference needs the analysis of the full CMB spectrum. However, in this case one aims to infer

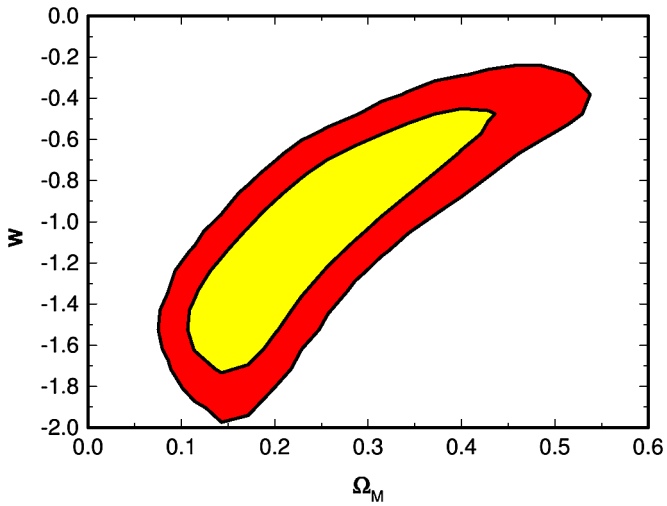

FIG. 4 (color online). Marginalized 1σ and 2σ likelihood contours inferred from the full WMAP 3-year spectra.

constraints from other data sets such as SN Ia or BAO and to include CMB information in a rapid and simple manner; the position of the CMB extrema provides a very efficient tool. In fact, while the CMB power spectrum analysis requires the solution of the Boltzmann equation for a given cosmological model, the evaluation of the position of the CMB peaks and dips is only a semianalytical computation. As an example, running publicly available Boltzmann codes [22] on a CPU at 2.3 GHz requires about one minute to compute the CMB spectra of a single model. Hence, using a MCMC sampling method, the evaluation of the full CMB likelihood requires about a few hours to reach full convergence of the MCMC chains, while using the CMB extrema only takes a few minutes.

In Fig. 3 (central upper panel) we extend our analysis of the CMB peaks and dips to nonflat models. Allowing for a nonvanishing curvature increases the geometric degeneracy and consequently leads to larger uncertainties in w. For instance, the 2σ marginalized constraints are $w < -0.34$ and $\Omega_K = -0.01 \pm 0.05$, respectively, and do not improve significantly under the HST prior.

The position of the CMB peaks and dips alone does not provide any insight on the time variation of dark energy. As it can be seen in Fig. 3 (right upper panel) the contours in the w_0- w_1 plane are spread over a large range of values. After marginalizing we find $w_0 < -0.55$ and $w_1 < 1.68$ at 2σ. It is worth mentioning that for increasing values of w_1, dark energy becomes dominant at earlier times. In such a case the presence of a non-negligible dark energy density at recombination modifies the position of the CMB peaks and dips primarily through its effect on the size of the sound horizon at decoupling. Therefore the location of the CMB extrema (after having accounted for the relative shifts) can put an upper bound on the time evolution of the equation of state at high redshifts (i.e. w_1). Our analysis shows that in order to be consistent with the observed peak structure, large positive values of $w_1 \gg 1$ are excluded (see also Sec. V). This is consistent with the fact that the analysis of the full CMB spectrum limits the amount of dark energy density at recombination to be less than 10% (otherwise it would strongly affect the amplitude and location of the CMB Doppler oscillations), hence providing a stringent upper bound on the value of the dark energy equation of state at early times (see [31,32]). In contrast, models with large negative values of $w_1 < 0$ leave no imprint at high redshifts, since in this case the dark energy density rapidly decreases for $z > 0$. Consequently, the likelihood remains unbounded in this region of the parameter space.

B. Combined constraints from CMB extrema and BAO

The baryon acoustic oscillations in the galaxy power spectrum provide a cosmic distance test at low redshifts. Therefore, in combination with CMB measurements they can significantly reduce the cosmological parameter degeneracies. In Fig. 3 (lower left panel) we plot the combined 1σ and 2σ contours in the Ω_m- w plane. At the 95% confidence level we find $\Omega_m = 0.12 \pm 0.12$ and $w < -1.10$, respectively. Imposing the HST prior further constraints the dark energy equation of state, $w < -1.14$. These results are compatible with those found in [13]. A model with $\Omega_m = 1$ is now excluded with a high confidence level since the combination of CMB extrema and BAO constrain the Hubble parameter in the range $h = 0.71 \pm 0.20$ at 2σ (see also [30]). Interestingly, the ΛCDM case ($w = -1$) appears to be on the edge of the 2σ limit, hence favoring nonstandard dark energy models. Indeed, unaccounted systematics effects in the BAO data can be responsible for such supernegative values of w. On the other hand, if confirmed this would provide evidence for an exotic phantom dark energy component [33] or could be interpreted as the cosmological signature of dark sector interactions (e.g. [34]).

The credible regions for nonflat models are shown in Fig. 3 (central lower panel). In this case we find $\Omega_K = -0.011 \pm 0.064$ and $w < -0.46$ at 2σ. These bounds do not change significantly under the HST prior. In Fig. 3 (lower right panel) we plot the 1σ and 2σ contours in the w_0- w_1 plane. Also in this case the bounds on a time varying dark energy equation of state remain large. For instance, we find the marginalized 2σ limits to be $w_0 < -0.74$ and $w_1 < 1.6$. Necessarily inferring tighter bounds on w_1 will require the combination of several other data sets, such as SN Ia luminosity distance measurements [35], which is the topic of next section.

V. CONSTRAINTS FROM SN IA

Here we want to compare the results derived in the previous section with limits inferred from luminosity distance measurements to SN Ia. We use the SN data set from the SNLS [14], and for simplicity, we limit our analysis to flat models. The results are summarized in Figs. 5 and 6, where we plot the 1σ and 2σ contours in the Ω_m-w and w_0-w_1 planes, respectively. The shaded regions correspond to limits inferred by combining the SN data with the location of the CMB extrema and assuming a hard prior on the baryon density and the scalar spectral index, $\Omega_b = 0.023$ and $n_s = 0.96$, respectively. We have verified that the constraints do not change significantly by assuming different prior parameter values.

Let us first focus on Fig. 5. We can see that the degeneracy line in the Ω_m-w plane is almost orthogonal to that probed by CMB and BAO, and indeed using the SN data requires external information to extract tighter constraints on dark energy. A common procedure is to assume a Gaussian prior on Ω_m consistently with the parameter inference from CMB and large scalar structure measurements, or alternatively to combine the SN analysis with BAO or the CMB shift parameter. Here we derive limits by combining the SN data with the position of the CMB peaks

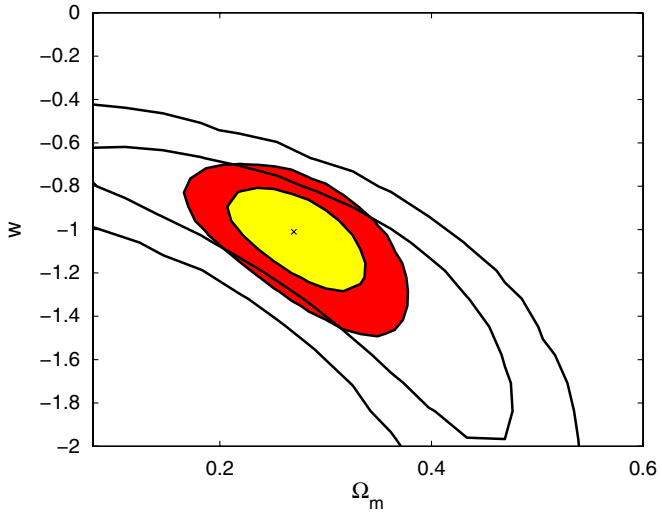

FIG. 5 (color online). Marginalized 1σ and 2σ contours in the Ω_m-w plane from SNLS data (solid lines) and in combination with the location of the CMB extrema (dark and light grey shaded regions).

and dips. This breaks the parameter degeneracy, thus providing smaller "credible" contours (shaded contours). In particular, after marginalizing, we find $\Omega_m = 0.24 \pm 0.11$ and $w = -1.01 \pm 0.29$ at 2σ, respectively. We can notice that these limits are only marginally consistent with those inferred using BAO in the previous section, thus indicating a potential discrepancy between the BAO measurements obtained in [13] and the SNLS data [14].

Let us now consider the case of a time varying equation of state. It is obvious that the parameter degeneracy between the matter density and the dark energy equation of state increases when additional equation of state parameters, which account for a possible redshift dependence, are included in the data analysis. This can be clearly seen in

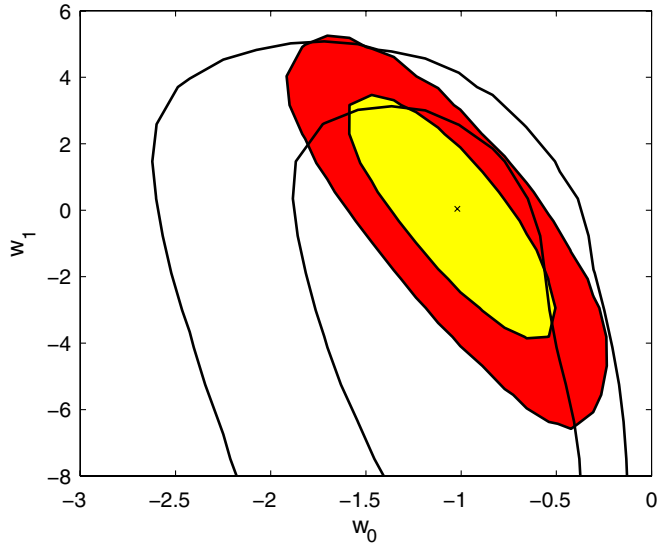

FIG. 6 (color online). As in Fig. 5 in the w_0-w_1 plane.

Fig. 6 were we plot the 1σ and 2σ contours in the w_0-w_1 plane. Nevertheless the SN data, differently from the case of BAO data in combination with CMB extrema (see lower left panel in Fig. 3), constrain w_0 in a finite interval. This is because SN Ia observations, by testing the luminosity distance over a range of redshift where the universe evolves from a matter dominated expansion to one driven by dark energy, are sensitive to at least one dark energy parameter (i.e. w or w_0) [36]. In such a case adding external information breaks the internal degeneracy and leads to finite bounds on both dark energy parameters. For instance, including the position of the CMB peaks and dips, the root-mean-square value and standard deviation for w_0 and w_1 derived from the MCMC chains are $w_0 = -1.04 \pm 0.33$ and $w_1 = -0.27 \pm 2.27$, respectively, the best fit model being $w_0 = -1.02$ and $w_1 = 0.04$. These results are consistent with those from other analyses in the literature (see e.g. [12]).

VI. SHIFT PARAMETER

The geometric degeneracy of the CMB power spectrum implies that different cosmological models will have similar spectra if they have nearly identical matter densities $\Omega_m h^2$ and $\Omega_b h^2$, primordial spectrum of fluctuations, and shift parameter $R = \sqrt{\Omega_m H_0^2} r_K(z_*)$ [37]. The authors of [12] have suggested that since l_a is nearly uncorrelated with R, then both parameters can be used to further compress CMB information and can be combined with other measurements in a user-friendly manner. For minimal extension of the dark energy parameters, the inferred values of R and l_a do not significantly differ from those inferred assuming the vanilla ΛCDM model [11,12]. Indeed, differences may arise if additional parameters, such as the neutrino mass, the running of the scalar spectral index, or tensor modes, are considered [11]. We extend this analysis to other models. In particular, by running a MCMC likelihood analysis of the full WMAP 3-year spectra, we infer constraints on R and l_a for models with an extra background of relativistic particles (characterized by the number of relativistic species, $N_{\rm eff} \neq 3$) [38], neutrino mass [39], a time varying equation of state parametrized in the form of CPL, and a dark energy component with perturbations characterized by the sound speed $c^2_{\rm DE}$. We also consider models with a running of the scalar spectral index, with a nonvanishing tensor contribution (see e.g. [40]) and, finally, with extra features in the primordial spectrum due to a sharp step in the inflaton potential as in [41].

As we can see from Table I the constraints on R and l_a are stable under minimal modifications of the dark energy model parameters; differences are smaller than a few percent, including the case of a clustered dark energy component ($c^2_{\rm DE} = 0$). In contrast, the confidence interval of l_a is shifted by a few percent in the ΛCDM model with the neutrino mass or an extra background of relativistic parti-

TABLE I. The 68% C.L. on the shift parameter R and the acoustic scale derived from the WMAP data. A top-hat age prior, 10 Gyrs $< t_0 <$ 20 Gyrs, is assumed.

Model	R	l_a
ΛCDM	1.707 ± 0.025	302.3 ± 1.1
wCDM($c^2_{\rm DE} = 1$)	1.710 ± 0.029	302.3 ± 1.1
wCDM($c^2_{\rm DE} = 0$)	1.711 ± 0.025	302.4 ± 1.1
ΛCDM$m_\nu > 0$	1.769 ± 0.040	306.7 ± 2.1
ΛCDM$N_{\rm eff} \neq 3$	1.714 ± 0.025	304.4 ± 2.5
ΛCDM$\Omega_k \neq 0$	1.714 ± 0.024	302.5 ± 1.1
$w(z)$CDM CPL($c^2_{\rm DE} = 1$)	1.710 ± 0.026	302.5 ± 1.1
ΛCDM + tensor	1.670 ± 0.036	302.0 ± 1.2
ΛCDM + running	1.742 ± 0.032	302.8 ± 1.1
ΛCDM + running + tensor	1.708 ± 0.039	302.8 ± 1.2
ΛCDM + features	1.708 ± 0.028	302.2 ± 1.1

cles, while the values of R are slightly modified for a running of the primordial power spectrum or the contribution of tensor modes. These results confirm previous analyses [11,12].

Although the values of R and l_a are nearly the same for the dark energy models we have considered, this should not be considered as an incentive to use these parameters without caution. For instance, there is no specific reason as to why one should use the values of R and l_a inferred from the vanilla ΛCDM, rather than those obtained accounting for the neutrino mass. Consequently, one may infer slightly different bounds on the dark energy parameters depending on whether neutrinos are assumed to be massless or not. Moreover, the reason that WMAP data constrain R and l_a to be nearly the same for simple dark energy models is because the effect of dark energy on the epoch of matter-radiation equality and the evolution of the density perturbations remain marginal. This might not be the case for other models, such as those for which the dark energy density is non-negligible at early times. Since this effect is not accounted for in the values of R and l_a inferred from the vanilla ΛCDM, their use may lead to strongly biased results. In contrast, the location of the CMB extrema is applicable to this class of models as well [18]. A similar consideration applies to inhomogeneous models in which the late time dynamics and geometry depart from that of the standard Friedmann-Robertson-Walker universe [42].

The applicability to models of modified gravity, such as the DGP scenario [43], deserves a separate comment. In these models, not only does the Hubble law differ from the standard ΛCDM, but also the evolution of the density perturbations can be significantly different. Therefore, unless the evolution of the linear perturbations is understood well enough as to allow for a precise calculation of the CMB and matter power spectra, the use of R and l_a, or alternatively of the position of the CMB extrema or the distance measurements from BAO might expose one to the risk of completely wrong results.

VII. CONCLUSIONS

The multipoles of the CMB extrema can be directly measured from the WMAP spectra and used to combine CMB information with other cosmological data sets. Corrections to the location of the CMB peaks and dips from prerecombination effects need to be taken into account for an unbiased parameter inference. Here we have shown that the position of the first peak as measured by WMAP 3-year data is strongly displaced with respect to the actual location of the acoustic horizon at recombination. This displacement is caused by gravitational driving forces affecting the propagation of sound waves before recombination. These effects are smaller on higher harmonics, indicating the presence of a scale dependent phase shift which becomes negligible on scales well inside the horizon.

We have performed a cosmological parameter inference using the position of the WMAP peaks and dips in combination with recent BAO measurements, and derived constraints on a constant dark energy equation of state under different model parameter assumptions.

The method we have presented here is an alternative to using the shift parameter R and/or the multipole of the acoustic horizon at decoupling l_a. We have tested for potential model dependencies of R and l_a by running a full CMB spectra likelihood analysis for different classes of models. Indeed, for simple dark energy models the inferred constraints on R and l_a do not differ from those inferred assuming the vanilla ΛCDM. Nevertheless, we have suggested caution in using these secondary parameters as *data*, since hidden assumptions may lead to biased results particularly when testing models which greatly depart from the ΛCDM cosmology.

Indeed, we do advocate the use of the full CMB spectra, particularly for constraining the properties of dark energy. In fact, more information on dark energy is encoded in the full CMB spectrum than just in the distance to the last scattering surface. Nevertheless, we think that using the location of the CMB extrema provides a fast and self-consistent approach for combining, in a user-friendly way, the CMB information with complementary cosmological data.

ACKNOWLEDGMENTS

P. S. C. is grateful to the Aspen Center for Physics for the hospitality during the ''Supernovae as Cosmological Distance Indicators'' Workshop where part of this work was developed. We are particularly thankful to Jean-Michel Alimi, Mauricio Calvao, Laura Covi, Michael Doran, Malcom Fairbarn, Jan Hamann, Martin Kunz, Julien Larena, Eric Linder, Yun Wang, and Martin White for discussions, suggestions, and help. We acknowledge the use of COSMOMC [44] for the analysis of the MCMC chains.

[1] P. De Bernardis *et al.*, Nature (London) **404**, 955 (2000); N. W. Halverson *et al.*, Astrophys. J. **568**, 38 (2002).
[2] M. C. Runyan *et al.*, New Astron. Rev. **47**, 915 (2003); C. L. Bennett *et al.*, Astrophys. J. Suppl. Ser. **148**, 1 (2003).
[3] G. Hinshaw *et al.*, Astrophys. J. Suppl. Ser. **170**, 288 (2007).
[4] A. D. Sakharov, JETP **49**, 345 (1965); J. Silk, Astrophys. J. **151**, 459 (1968); P. J. E. Peebles and I. T. Yu, Astrophys. J. **162**, 815 (1970).
[5] N. Vittorio and J. Silk, Astrophys. J. Lett. **285**, L39 (1984); J. R. Bond and G. Efstathiou, Astrophys. J. Lett. **285**, L45 (1984); A. G. Doroshkevich, Sov. Astron. Lett. **14**, 125 (1988).
[6] W. Hu and N. Sugiyama, Phys. Rev. D **51**, 2599 (1995).
[7] W. Hu and M. White, Astrophys. J. **471**, 30 (1996).
[8] M. Kamionkowski, D. N. Spergel, and N. Sugiyama, Astrophys. J. Lett. **426**, L57 (1994).
[9] D. N. Spergel *et al.*, Astrophys. J. Suppl. Ser. **170**, 377 (2007).
[10] D. J. Eisenstein, W. Hu, and M. Tegmark, Astrophys. J. Lett. **504**, L57 (1998).
[11] O. Elgaroy and T. Multamaki, Astron. Astrophys. **471**, 65 (2007).
[12] Y. Wang and P. Mukherjee, Phys. Rev. D **76**, 103533 (2007).
[13] W. J. Percival *et al.*, Mon. Not. R. Astron. Soc. **381**, 1053 (2007).
[14] P. Astier *et al.*, Astron. Astrophys. **447**, 31 (2006).
[15] W. Hu and N. Sugiyama, Astrophys. J. **444**, 489 (1995).
[16] M. J. Rees and D. W. Sciama, Nature (London) **217**, 511 (1968).
[17] W. Hu, M. Fukugita, M. Zaldarriaga, and M. Tegmark, Astrophys. J. **549**, 669 (2001).
[18] M. Doran and M. Lilley, Mon. Not. R. Astron. Soc. **330**, 965 (2002).
[19] L. Page *et al.*, Astrophys. J. Suppl. Ser. **148**, 233 (2003).
[20] R. Keskitalo *et al.*, J. Cosmol. Astropart. Phys. 09 (2007) 008.
[21] J. Magueijo *et al.*, Phys. Rev. Lett. **76**, 2617 (1996).
[22] U. Seljak and M. Zaldarriaga, Astrophys. J. **469**, 437 (1996); A. Lewis, A. Challinor, and A. Lasenby, Astrophys. J. 538, 473 (2000); M. Doran, J. Cosmol. Astropart. Phys. 10 (2005) 011.
[23] W. Hu and N. Sugiyama, Astrophys. J. **471**, 542 (1996).
[24] P. S. Corasaniti and E. J. Copeland, Phys. Rev. D **65**, 043004 (2002).
[25] M. Doran, M. Lilley, and C. Wetterich, Phys. Lett. B **528**, 175 (2002).
[26] S. Sen and A. A. Sen, Astrophys. J. **588**, 1 (2003).
[27] M. Chevallier and D. Polarski, Int. J. Mod. Phys. D **10**, 213 (2001).
[28] E. V. Linder, Phys. Rev. Lett. **90**, 091301 (2003).
[29] W. L. Freedman *et al.*, Astrophys. J. **553**, 47 (2001).
[30] P. Hunt and S. Sarkar, Phys. Rev. D **76**, 123504 (2007).
[31] R. R. Caldwell and M. Doran, Phys. Rev. D **69**, 103517 (2004).
[32] P. S. Corasaniti *et al.*, Phys. Rev. D **70**, 083006 (2004).
[33] R. R. Caldwell, M. Kamionkowski, and N. N. Weinberg, Phys. Rev. Lett. **91**, 071301 (2003).
[34] S. Das, P. S. Corasaniti, and J. Khoury, Phys. Rev. D **73**, 083509 (2006).
[35] G.-B. Zhao *et al.*, Phys. Lett. B **648**, 8 (2007).
[36] E. V. Linder and D. Huterer, Phys. Rev. D **72**, 043509 (2005).
[37] J. R. Bond, G. Efstathiou, and M. Tegmark, Mon. Not. R. Astron. Soc. **291**, L33 (1997).
[38] R. Bowen, S. H. Hansen, A. Melchiorri, J. Silk, and R. Trotta, Mon. Not. R. Astron. Soc. **334**, 760 (2002); S. H. Hansen *et al.*, Phys. Rev. D **65**, 023511 (2001).
[39] G. L. Fogli *et al.*, Phys. Rev. D **75**, 053001 (2007); **70**, 113003 (2004).
[40] W. H. Kinney, E. W. Kolb, A. Melchiorri, and A. Riotto, Phys. Rev. D **74**, 023502 (2006).
[41] L. Covi, J. Hamann, A. Melchiorri, A. Slosar, and I. Sorbera, Phys. Rev. D **74**, 083509 (2006); J. Hamann, L. Covi, A. Melchiorri, and A. Slosar, Phys. Rev. D **76**, 023503 (2007).
[42] J. Larena *et al.* (unpublished).
[43] G. R. Dvali, G. Gabadadze, and M. Porrati, Phys. Lett. B **485**, 208 (2000); C. Deffayet, Phys. Lett. B **502**, 199 (2001).
[44] A. Lewis and S. Bridle, Phys. Rev. D **66**, 103511 (2002).